Interfacial structure in (111) Au:Ni multilayers investigated by anomalous x-ray diffraction

T. Bigault, F. Bocquet, S. Labat, and O. Thomas
TECSEN, CNRS, Faculté des Sciences de Saint Jérôme, 13397 Marseille Cedex 20, France

H. Renevier
Laboratoire de Cristallographie, CNRS, 25 Avenue des Martyres, BP 166 X, 38042 Grenoble Cedex, France
(Received 16 February 2001; published 10 September 2001)

We have investigated the structure of buried interfaces in (111) Au:Ni multilayers. Conventional x-ray diffraction at constant energy as well as anomalous x-ray scattering across the Ni absorption *K* edge have been used. Whereas the fitting of the spectra at a single energy leads to two different possible interfacial structures, the anomalous diffracted intensity variation unambiguously favors a model with an interfacial concentration gradient at one interface. The multilayer presents an intermixed region extending on six atomic planes around the Ni/Au interface, whereas the Au/Ni interface is chemically abrupt. This structure can explain the unusual stress-strain relation previously reported on this system.

DOI: 10.1103/PhysRevB.64.125414 PACS number(s): 68.35.Dv

I. INTRODUCTION

Metallic multilayers, with periods in the nanometer range, present novel properties compared to mixtures (e.g., magnetic, magneto-optic, transport, etc.). The average properties of these layered systems are expected to be related to the structure of the interfaces. A rather large number of experimental and theoretical studies have been devoted to the transition from a coherent interface to an incoherent one,[1,2,3] driven by the elastic energy stored in the layer. In the case of nanometric films, the mechanisms at work still raise fundamental questions[4] since the film thickness is comparable to the dislocation core radius. Many fewer studies[5] focus on the chemical gradients that may exist close to interfaces. It is seldom realized that interfacial mixing may be a way to decrease the elastic energy[6] in a lattice parameter-mismatched system.

In this work we have studied in detail the interfacial structure in (111) Au:Ni multilayers. The Au-Ni system has been the object of many investigations for many years. The size difference between these two elements is huge (14%) and thought to be responsible[7] for the large miscibility gap present in the equilibrium[8] phase diagram. The difference between Au and Ni is also apparent when one looks for (111) surface energies[9] ($\gamma^{Au}=1.333\,J\,m^{-1}$, $\gamma^{Ni}=2.080\,J\,m^{-1}$) or for elastic constants[10] [(111) biaxial moduli: $Y^{Au}=189\,GPa$, $Y^{Ni}=390\,GPa$]. In a previous study,[11] we have investigated the lattice parameters of Au and Ni in different (111) multilayers. It was found that the Au lattice is under compression and that the deformation state of the unit cell can be described in a purely elastic framework. At variance with this behavior, the Ni lattice exhibits an isotropic expansion that was attributed[11] to the presence of Au in the Ni sublayers. Similar findings have been reported by other groups,[12–14] although some authors attributed the deformation of Ni to a negative Poisson ratio.[14] Moreover, the discrepancy between stress and strain measured *in situ* during the growth[15] pointed also to the occurrence of mixing. Finally, it is important to underline that all the studies reported so far agree on the highly asymmetric behavior of the system: a purely elastic behavior in Au and an isotropic lattice expansion in Ni. Nevertheless, and until now, Au mixing was only hypothesized. Indeed, all these studies were based on interplanar distance measurements, so no direct chemical evidence for the Au:Ni interfacial mixture was obtained. One should quote, however, the study by Bayle *et al.*[16] where electron energy loss spectroscopy (EELS) studies on ⟨001⟩ Au:Ni multilayers indicated mixing at the Ni/Au interface.

The purpose of this study is twofold: (1) to get direct ''chemical'' evidence for the presence of Au in the Ni layers, in the as-grown (111) multilayers, and (2) to obtain more detailed information on the interfacial composition and strain gradients, compared to the average one deduced from Bragg peak positions. To fulfill these objectives we present a simulation of diffracted intensities combined with x-ray anomalous scattering. We have used the anomalous x-ray scattering effect around the Ni absorption *K* edge (8333 eV) since the chemical information from the interface is expected to be more important using the Ni edge rather than the Au one (11 919 eV). Indeed, the multilayer that has been studied here is Au rich with a thickness ratio Au:Ni=3:1. Thus, in proportion, there are more Ni atoms close to interfaces than Au ones. It is well established that x-ray anomalous scattering provides information from spatially distinct regions of a multilayer[17–21] when the sample contains atoms whose absorption edges are sufficiently separated in energy. Moreover, anomalous x-ray scattering[22] is a powerful method to investigate the local chemical nature in order to separate at the nanometric scale a mixed film (solid solution) from a stack of films with similar cell parameters (multilayer). In conclusion, anomalous x-ray scattering is a technique perfectly adapted for our purpose, i.e., to investigate the structure of buried interfaces in Au:Ni multilayers.

This paper is organized as follows. Section II describes the experimental procedure. In Sec. III the analysis of symmetric $\theta/2\theta$ x-ray diffraction (XRD) scans is reported. Two clearly different structures, both in agreement with XRD data, are derived: one with interfacial mixing and another one with chemically abrupt interfaces. No reliable information on the actual chemical nature of the interface could be

extracted. In Sec. IV we show how a semiquantitative anomalous data analysis removes the latter indetermination. The oscillatory part of the signal, which contains the x-ray absorption fine structure information on the short-range order, is not analyzed in this paper. This diffraction anomalous fine structure (DAFS) study lies on a more complex fitting process[23] and will be done in a further work.

II. EXPERIMENT

The 21-period (111) Au:Ni multilayers were grown by molecular beam epitaxy on a 500-Å-thick (100) Cu buffer layer deposited on a (100) Si wafer. The samples were capped with a gold layer. More details[11] on the growth can be found elsewhere. The nominal superlattice period is 40 Å. One bilayer is nominally made of a 30-Å-thick gold layer and a 10-Å-thick nickel layer. The thickness was monitored with a quartz oscillator during growth. First, an XRD analysis was performed with a laboratory apparatus. The measured total multilayer thickness is 850 Å, in agreement with the expected one. The coherence length in the growth direction is at least about 500 Å, estimated from the width of the 1° peak (see Sec. III). A strong ⟨111⟩ texture axis[11] with four variants {(111)⟨110⟩Au,Ni‖(100)⟨110⟩Cu} occurs. The mosaicity around the texture axis is about 4°.

Experiments were carried out at the beamline D2AM, which is dedicated to anomalous scattering analysis,[24] at the European Synchrotron Radiation Facility (ESRF) in Grenoble, France. The seven-circle diffractometer available at D2AM was used to put the ⟨111⟩ texture axis in the diffraction plane (with tilt angle χ). We performed all the measurements with momentum transfer q normal to the interfaces of the multilayer (symmetric scans). Data were collected with the x-ray polarization vector normal to the scattering plane. All the angular motions have a resolution lower than 0.001°. The incoming monochromatic beam intensity I_0 was measured with a scintillator using the scattering of a thin film of Kapton. A 1-mm slit in front of the detector (in the 2θ direction) improves the resolution and reduces the fluorescence background during the diffraction data acquisition. High-energy resolution (a few eV corresponding to $\Delta E/E \approx 2\times10^{-4}$) and high-$q$ resolution ($\Delta q/q \approx 10^{-3}-10^{-4}$) are achieved.

On D2AM we performed two different kinds of experiments: (1) conventional XRD $\theta/2\theta$ symmetric scans at different, but fixed during the scans, energies and (2) top-DAFS scans (i.e., intensity measurements at a constant q, corresponding to the peak top position, as a function of energy). In the case of $\theta/2\theta$ experiments, the symmetric scans and the fluorescence signal were recorded with a 500-Å-thick silicon photodiode in photovoltaic mode. In the case of DAFS experiments, the Bragg peak tracking versus energy was performed using a linear regression for $\sin\theta(1/E)$ obtained by a diffraction preexperiment to find peak positions at several energies in the range 8200–8800 eV (i.e., around the Ni edge which lies at 8333 eV). To track the position of the different Bragg peaks, the characteristics of D2AM were sufficient because the superlattice peaks were broad enough [full width at half maximum (FWHM) around 0.4° or $\Delta q \approx 5\times10^{-2}$].

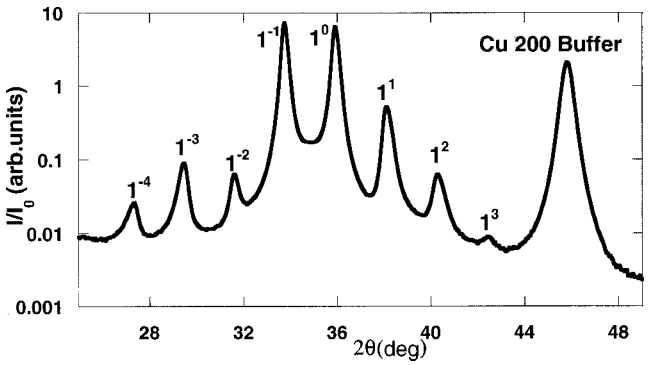

FIG. 1. Raw data normalized by the incoming intensity I_0 of a symmetric scan of the Au/Ni multilayer recorded at $E=8215$ eV.

The fluorescence signal and DAFS spectra were recorded with a NaI scintillator or with a photodiode (depending on the intensity). During the DAFS measurements, the fluorescence signal was recorded near the considered superlattice peak (with a χ shift of about 6°) to maintain geometrical conditions close to the diffraction ones. It was important to keep the same recording geometrical conditions because the experimental fluorescence was used for the absorption correction of the DAFS spectra.

III. QUANTITATIVE ANALYSIS OF THE $\theta/2\theta$ SYMMETRIC SCANS

In multilayers when the coherent domain size is larger than the superperiod Λ, the peak positions are given by $2\sin\theta_n = n\lambda/\Lambda$, where n is an integer, θ_n the Bragg angles, and λ the wavelength. For convenience, the high-angle peak positions are usually indexed about the average interplanar distance $\bar{d}=\Lambda/(N_{\mathrm{Ni}}+N_{\mathrm{Au}})$ where N_{Ni} and N_{Au} are the number of atomic planes of Ni and Au, respectively, in one unit cell (one bilayer):

$$\frac{2\sin\theta_n}{\lambda}=\frac{p}{\bar{d}}\pm\frac{n}{\Lambda}.$$

Here p labels the order of the peak related to the average distance and n labels the order of the satellite around the average Bragg peak. In our case (see Fig. 1), $p=1$ because we present first-order symmetric spectra. Without any simulation, $\bar{d}$ and Λ may be directly extracted from the data. With a linear regression on the positions of the satellite peaks, we extracted $\Lambda=38.7\pm0.3$ Å in agreement with the nominal superperiod. $\bar{d}$ was precisely determined from the position of the 1° peak. $\bar{d}$ is 2.27 ± 0.02 Å. The individual lattice parameters, the number of atomic planes, the interfacial chemical composition, and the disorder require fine modeling. Fits in agreement with the experimental relative intensities of the different peaks and with the global line profile of the first order $\theta/2\theta$ scans were derived. This procedure allows the determination of the average cell and the deviation[25] from this average. $\theta/2\theta$ experiments were recorded at 8215, 8315, and 8415 eV.

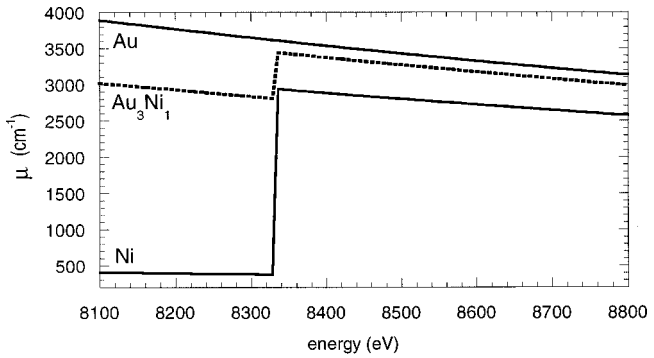

FIG. 2. Absorption coefficient for Au, Ni, and the Au:Ni multilayer. The absorption of the multilayer is an average of the pure material ones weighted by the respective thickness ratio of the materials in the multilayer.

A. Intensity normalization

All the data were normalized by the incoming intensity I_0. The normalized fluorescence intensity was subtracted from the normalized diffracted intensity. Spectra recorded at different energies were first normalized with respect to each other by using the peak intensity of the Cu buffer layer (corrected for absorption from the multilayer) as reference. The experimental $I^{\mathrm{expt}}(q,E)$ intensity, where q is the momentum transfer vector and E the energy, is proportional to the structure factor $F(q,E)$ squared:

$$I^{\mathrm{expt}}(q,E)=|F(q,E)|^2K(E)\mathrm{LP}(q,E)A(q,E). \qquad (1)$$

Here K represents a global experimental scaling factor. Its small variation with energy does not depend on the anomalous variation of the atomic scattering factor. The contribution of $K(E)$ was eliminated with the normalization using the Cu peak. $\mathrm{LP}(q,E)$ is the Lorentz-polarization correction. The polarization vector was normal to the scattering plane during experiments, so the polarization correction was unity. The Lorentz correction in this geometry is $1/(E^3\sin 2\theta)$. Here $A(q,E)$ is the absorption correction multiplied by the exposed area factor. The absorption correction is calculated by integrating over the different possible path lengths in the multilayer of thickness e. In symmetrical reflection, $A(q,E)$ is

$$A(q,E)=\frac{1-\exp\left(\dfrac{-2\mu(E)e}{\sin\theta}\right)}{\dfrac{2\mu(E)}{\sin\theta}}\frac{1}{\sin\theta}, \qquad (2)$$

where $\mu(E)$ is the average linear absorption coefficient combining resonant (Ni) and nonresonant (Au) atoms. $\mu(E)$ is calculated with the atomic absorption of Ni and Au (Ref. 26) and the nominal thickness ratio Au:Ni=3:1. The absorption coefficient variation with energy is shown in Fig. 2. Normalized spectra are shown in Fig. 3. The anomalous intensity variation modifies only slightly the global scan profile. As one can see, only the 1^{+2} satellite is clearly modified. But the contribution of these peaks to the global fitting is weak (the intensity is two or three orders of magnitude smaller than the main peaks). Therefore, we present fits only for $E=8215$ eV because the best refinement done at other energies gave the same structural parameters.

B. Fitting procedure and results

The purpose of this section is to extract information on the interfacial structure by performing fittings of the $\theta/2\theta$ scans. We have focused on the possible occurrence of interfacial mixing by determining the composition profile at each interface. We chose to perform quantitative analyses of the spectra with the superlattice refinement by x-ray diffraction[25] (SUPREX) program version 9.0. A general kinematical diffraction one-dimensional (1D) formula, which includes continuous and discrete fluctuations from the average structure (in the growth direction), is used in SUPREX. The plane scattering factors were calculated by multiplying the density by the atomic scattering factor of the in-plane material. The scattering factor of a mixed plane was calculated assuming a simple rule of mixture considering the in-plane concentration of Ni and Au. The nonanomalous part of atomic scattering factors and their variations with q are tabulated in SUPREX's librar-

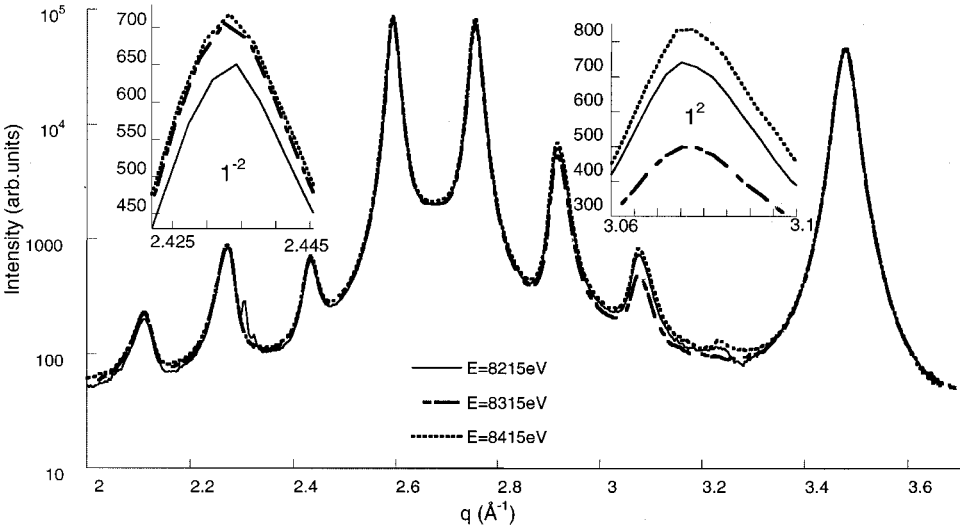

FIG. 3. Symmetric scans at 8215, 8315, and 8415 eV in logarithmic scale. The data have been first normalized with respect to each other using the Cu peak. Absorption and Lorentz corrections have also been performed. The two insets are enlargements of the 1^2 and 1^{-2} peaks in linear scale.

TABLE I. Best-fit concentration and interplanar distance profiles for the two models (a) and (b) from data at $E=8215$ eV. Only the profile for the Ni/Au interface is described. See the text for the parameters and model signification. The table has to be read from the left to the right, which corresponds to the growth direction. Only the region affected by the interface presence is shown in the table. The other interplanar distances are d_{Au}, and the other in-plane concentrations are 100% in the Au-rich layer.

	d_{Au} / d_{Ni} (Å)	d_{int} / σ_{int} (Å)	N_{Au} / σ_{Au}	N_{Ni} / σ_{Ni}	Au-rich layer profile Au concentration (%) Interplanar distance (Å)	Ni-rich layer profile Ni concentration (%) Interplanar distance (Å)
Model (a)	2.373	2.16	11.95	4.9	..., 100; 100; 100; 100	100; 100; 100; 100
	2.095	0.15	0.96	0.1	..., 2.37, 2.368, 2.34, 2.17	2.14, 2.12, 2.10, 2.08
Model (b)	2.371	2.22	11.8	5.09	..., 100, 82.7, 60.9	60.9, 82.7, 100
	2.066	0.14	0.9	0.06	..., 2.37, 2.352, 2.285	2.16, 2.086, 2.066

ies. We added the anomalous part given by Sasaki[27] to the libraries. The mean parameters describing the structure are the following: N, the number of deposited periods fixed at 21 in our case; d_{Ni} and d_{Au}, the interplanar distance in the region far from the interfaces in the Ni and Au layers; N_{Ni} and N_{Au}, the number of planes, allowed to be noninteger, in the Ni and Au layers; and $d^{\mathrm{int}}_{\mathrm{Au\text{-}Ni}}$ and $d^{\mathrm{int}}_{\mathrm{Ni\text{-}Au}}$, the interfacial distances at the interface Au/Ni and Ni/Au, respectively.[28] The influence of these parameters on the diffraction spectra is important, but their physical meaning is difficult to understand. We chose to fix $d^{\mathrm{int}}_{\mathrm{Au\text{-}Ni}}$ and $d^{\mathrm{int}}_{\mathrm{Ni\text{-}Au}}$ as an average between the last interplanar distance in Au and Ni, respectively, layer and the first interplanar distance in the Ni and Au layers, respectively.

In SUPREX, two different models exist to describe chemical and/or structural modifications (around d_{Ni} and d_{Au}) in the regions influenced by the interface. In the first one [called model (a) in the following], an adjustable exponential gradient of interplanar distances is allowed. This gradient extends on three planes on each side of the interfaces and can be fixed independently at the Au/Ni and Ni/Au interfaces. A composition profile, uncorrelated with the latter gradient profile, extending exponentially on three planes on each side of the interfaces, may also be introduced. Nevertheless, in this (a) model, the chemical profiles of the intermixed regions are exactly the same at the Au/Ni and Ni/Au interfaces. Interfaces chemically asymmetric are not available in this model. The second model [called model (b) in the following] combines simultaneously a composition and a distance profile. The interplanar distance gradient is linearly linked to the composition profile by assuming a simple rule of mixture. The concentration profile is linear, symmetric, and extends on N^{mix} atomic planes around the interface. In this (b) model, the Au/Ni and Ni/Au interfaces can be described independently by two distinct adjustable parameters $N^{\mathrm{mix}}_{\mathrm{Au\text{-}Ni}}$ and $N^{\mathrm{mix}}_{\mathrm{Ni\text{-}Au}}$. No intralayer fluctuations or static Debye-Waller factors are considered. Cumulative layer thickness fluctuations, because they imply fluctuations of the superperiod,[29] are very important for the relative intensities of the peaks and for their broadening. This disorder is included in the SUPREX formula, which considers random and independent fluctuations in each layer. Two parameters are used: σ_{Ni} and σ_{Au} being the rms of a discrete Gaussian distribution around N_{Ni} and N_{Au}. Interfacial disorder is simulated with a continuous Gaussian distribution (rms: σ_{int}) around d^{int}. The combined effects of σ_{int}, σ_{Ni}, and σ_{Au} can be related to the interfacial roughness and to the loss of coherency in the growth direction.

We performed the fitting procedure as follows: First, fitting of N_{Ni}, N_{Au}, d_{Au}, and d_{Ni} to reproduce exactly the peaks positions. Then we fitted the different disorder parameters to describe the broadening. To finish, we performed refinements with all parameters free for the different models available in SUPREX. To reproduce exactly the profile and relative intensities, the fitting procedure converges to a gradual structure in the layers with two different interfaces. Two satisfying models [models (a) and (b)] are obtained and detailed in Table I. Figure 4 presents a graphic representation of the (b) model. Figure 5 shows the agreement between the two fits and the experimental data. The Au/Ni interface is chemically abrupt (no intermixing) in models (a) and (b). The distance profile at the interface Au/Ni is, for the Au layer, exactly abrupt in model (b), while the first Au interplanar distance is expanded (0.17 Å) in model (a). The Ni/Au interface presents a distance gradient and no intermixed region in model (a). In model (b), the Ni/Au interface presents an intermixed region and a coupled distance gradient. The agreement factor χ^2 is calculated using the following formula:

$$\chi^2=\frac{1}{N_{\mathrm{pts}}}\sum_{1}^{N_{\mathrm{pts}}}(\ln I_{\mathrm{cal}}-\ln I_{\mathrm{meas}})^2.$$

Here $\chi^2=8\times10^{-3}$ for model (a) and $\chi^2=7\times10^{-3}$ for model (b). The χ^2, achieved using the (b) model, is not significantly better than the one achieved using the (a) model. The number of adjustable parameters is smaller in model (b) than in model (a). So it seems that model (b) is better than model (a), but no real quantitative arguments are available to choose between the two models.

The mean interplanar distance in the Au layers is for the two models 2.355 ± 0.005 Å in agreement with the value[11] deduced from asymmetric XRD measurements. For both models, the mean interplanar distance in the Ni layers was

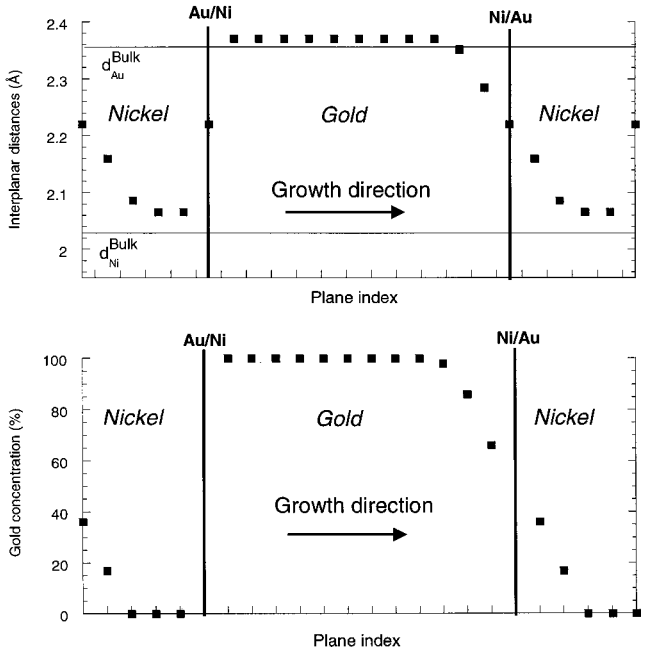

FIG. 4. Graphic representation of the (b) model (see also Table I). Top: representation of the evolution of the interplanar distances in a bilayer. Bottom: representation of the evolution of the gold concentration in a bilayer. Note the position of the interfaces and the respective notation used to describe the interfaces.

found to be 2.10 ± 0.01 Å [compared to the bulk distance (2.034Å)]. Ni is largely expanded in the growth direction as previously reported. In model (b), the intermixed region extends on 4.6 planes (the N^{mix} parameter). The quantity of Au involved in the intermixing is equivalent to two planes. Using a different calculation procedure and assuming *a priori* some intermixing, Gladyszewski *et al.*[30] performed an analysis of the symmetric scan on a similar sample. Their simulation concluded that the intermixed quantity of Au is equivalent to the 1.5 plane in agreement with our previous[11] results. We also obtained disorder parameters given by the rms value in SUPREX. These rms values are important and linked to the

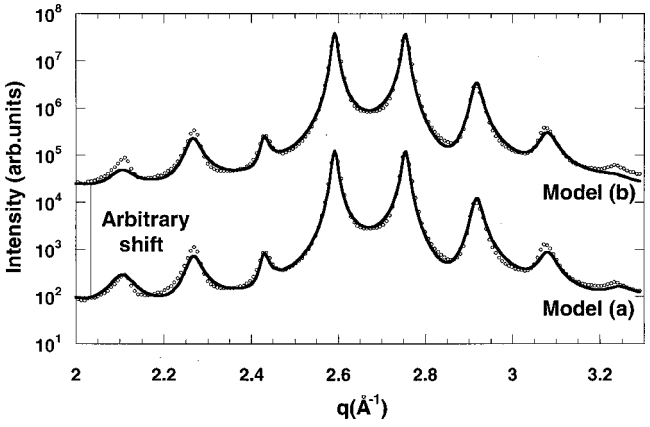

FIG. 5. Comparison between fits (in solid line) and data (open circle) recorded at $E = 8215$ eV. Model (a): deformation around the interfaces is allowed. Model (b): deformation and intermixing around the interfaces are allowed.

interfacial roughness. X-ray reflectivity[31] also indicates an important correlated and cumulative roughness in the growth direction. Models (a) and (b) are consistent with all previous works done on this system.

The simulations presented in this section, even if they are in good agreement with experimental data, do not allow any clear conclusion on the chemical nature of the interface. A global fitting procedure (even if it is improved) including the disorder parameters of the multilayer does not seem to be a good way to remove the indetermination on the structure. Therefore, we chose to focus only on the average structure that one can extract from top-DAFS measurements through the Ni absorption *K* edge.

IV. ANALYSIS OF X-RAY ANOMALOUS SCATTERING DATA

This technique exploits the high sensitivity, with energy and momentum transfer vector, of the diffracted intensity. In a kinematic 1D approximation, the diffracted intensity $I(E,q)$ of a perfect multilayer is given by the structure factor $F(E,q)$ squared:

$$I(E,q) = \left| \sum_i \left(c^i_{\mathrm{Au}} \rho_{\mathrm{Au}} f_{\mathrm{Au}}(E,q) + c^i_{\mathrm{Ni}} \rho_{\mathrm{Ni}} f_{\mathrm{Ni}}(E,q) \right) \exp(jq.d_i) \right|^2, \qquad (3)$$

where d_i, c^i, and ρ are the interplanar distance between the i and $i+1$ planes, the concentration in the i plane, and the density of each material, respectively. $f_i(E,q) = f_i^0(q) + f_i'(E) + j f_i''(E) + \Delta f_i''(E)\chi(E)$ is the atomic scattering factor. In $f_i(E,q)$, the first term is the Thomson scattering factor. The second and third ones are the resonant and antiresonant corrections, respectively, as for a single isolated atom. The last oscillating term is small compared to the other ones. $\chi(E)$ is produced by the neighboring atoms[23] and contains XAFS-like information. The variable resonant contribution in $F(E,q)$ around the Ni *K* edge provides a way to modulate the ''Ni chemical weight'' in the diffracted intensity. The strong intensity dependence on q (i.e., the satellite order), arising from the d and q coupling in $F(E,q)$, gives a spatially resolved sensitivity. Due to the two combined effects, anomalous x-ray scattering is a fine spatial chemical probe.

A. Simulation

In this part, we focus on simulation of the nonoscillating part of the intensity variations with energy at a constant q (corresponding to the peak maximum) for each satellite peak. To simulate these experimental variations, the sample structure was described plane by plane (i.e., an in-plane chemical composition for each plane and each interplanar distance) in one bilayer. The number of atomic planes is thus an integer. This description takes into account the distance and/or the composition modifications close to the interfaces, compared to the regions far from the interfaces. Nevertheless, no disorder parameters (i.e., static Debye Waller factors, layer

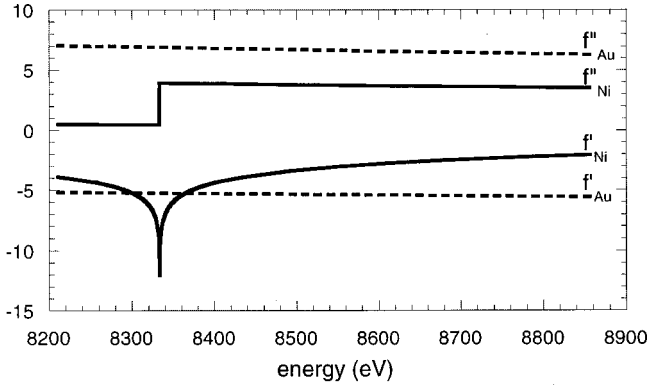

FIG. 6. Real part (f') and imaginary part (f'') of the Ni and Au atomic scattering factors.

thickness cumulative or noncumulative fluctuations, interfacial distance fluctuations) were considered.

By using this simple description of the structure, we implicitly assumed that the disorder effects do not affect the intensity anomalous variations. Nevertheless, the understanding of the actual influence of disorder on the intensity anomalous variation is a difficult task. Experimentally,[18] by studying the relative variation of the peak intensity, it was assumed that the influence of many disorder parameters might be eliminated. This assumption is clearly true if the effect of disorder can be treated as a multiplying factor, independent of energy, in the structure factor. Sevenhans *et al.*[29] showed that a cumulative or a noncumulative layer thickness fluctuation may be described with the latter formalism. On the contrary, Proietti *et al.*[32] showed that the Debye-Waller factors, which have an important effect on the DAFS spectra, could not be simply described by a multiplying factor. In this latter study, the different Debye-Waller factors were found to be correlated and had to be fitted, with the other structural parameters, in the structure factor. *A priori*, in the Au-Ni multilayers all the different kinds of latter disorders have to be considered, and it is difficult to conclude on their influences on the DAFS spectra. Nevertheless, we attempted to clarify this point via an empirical approach using the experimental data. It is well known that the disorder effect is very important on peak broadening. If the width of each peak is constant with energy, one can interpret the observed top intensity variation without considering any disorder-dependent anomalous effect. Thus we measured the width of several peaks on the symmetric $\theta/2\theta$ scans recorded at 8215, 8315, 8415, and 8815 eV. The shape of the peaks, including their mutual overlapping, was fitted by a pseudo-Voigt function with very good agreement. We found that the width of all the peaks varied less than 5.5% in $q(\text{Å}^{-1})$. The peak widths are roughly constant with energy; thus, one can conclude, *a posteriori*, that the disorder describing the Au/Ni multilayers does not modify the anomalous intensity variations. A more theoretical treatment of the influence of disorder on DAFS spectra would be interesting, but is out of the scope of this paper.

Our purpose is to distinguish between an abrupt and an intermixed interface with different models that do not include disorder. We calculated the intensity variations of the peaks with two simple models (a′) and (b′). The distance

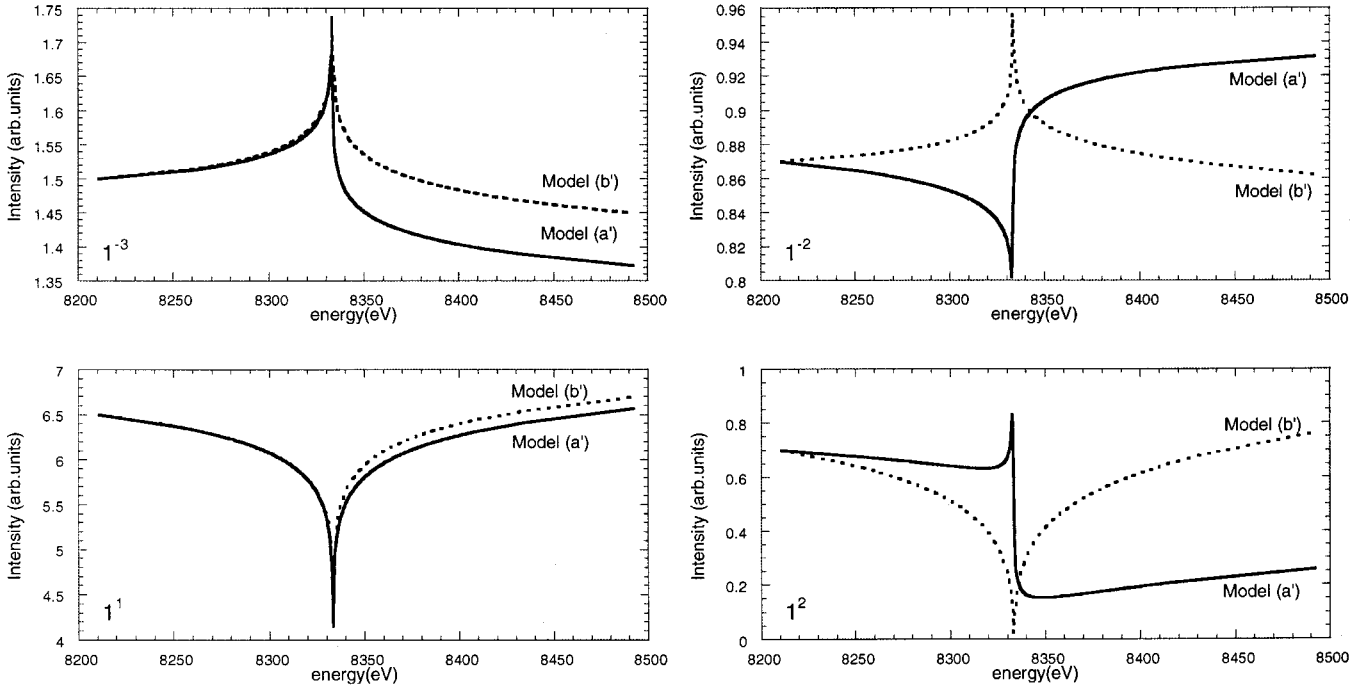

FIG. 7. Simulation of the anomalous variation of the intensity at the top of different peaks. Model (a′) refers to a simplified model (a) (no disorder and deformation *without* intermixing around the Ni/Au interface). Model (b′) refers to a simplified model (b) (no disorder and deformation *with* intermixing around the Ni/Au interface). Intensity is normalized to match the experimental one at $E=8200$ eV. Notice the clearly different shapes of the 1^2 and 1^{-2} peaks in models (a′) and (b′).

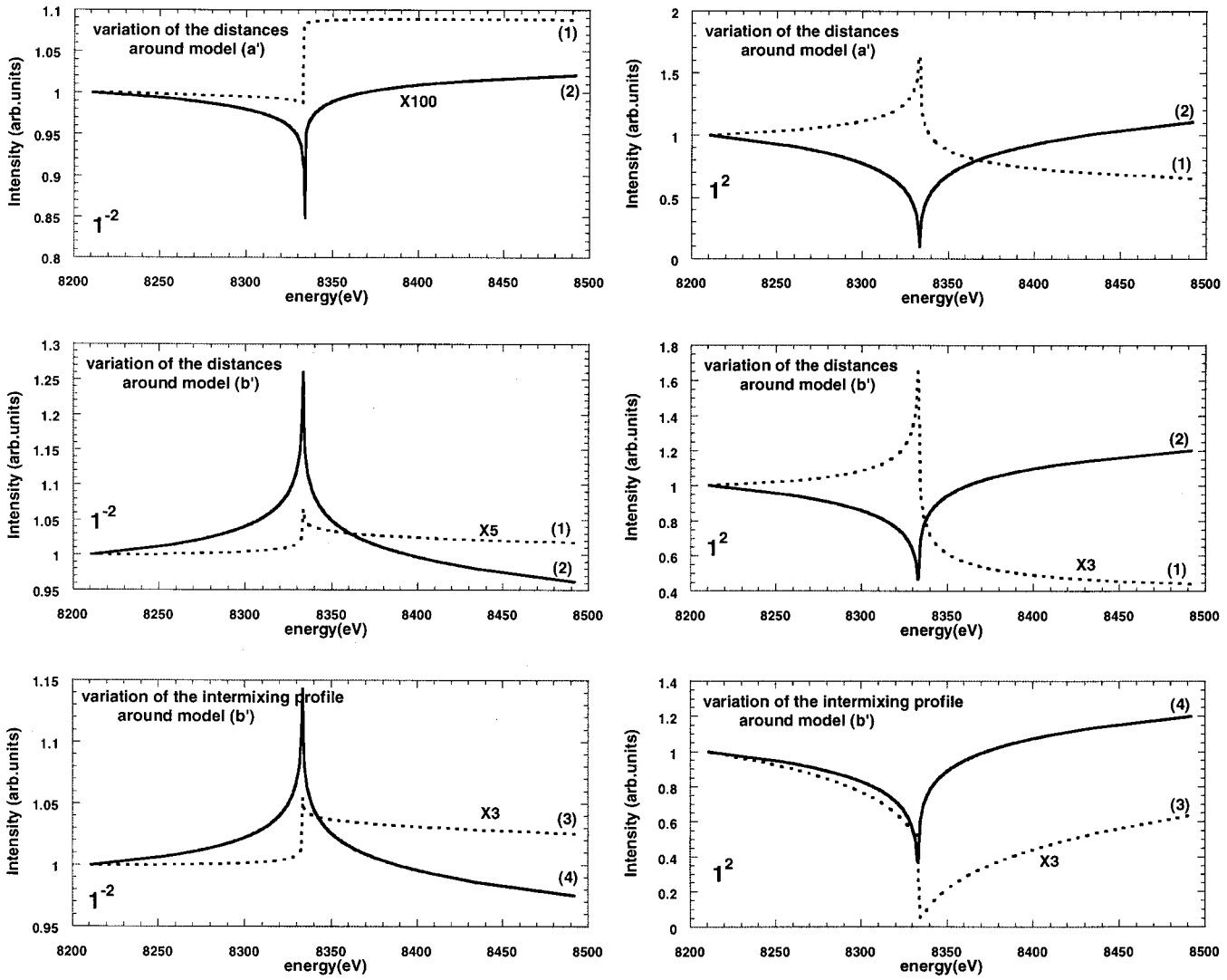

FIG. 8. Shape of the anomalous variation of the Bragg peaks intensity with modifications of the structure around models (a′) and (b′). (1) Maximum deformation around interface (see text); (2) minimum deformation around interface (see text); (3) intermixed zone equivalent to one plane on each side of the interface; (4) intermixed zone equivalent to four planes on each side of the interface. Simulated intensities are arbitrarily normalized to the one at $E=8200$ eV. For each comparison, when the intensities are strongly different, the factor to adjust the smallest in the range of the largest is mentioned.

gradient at a Ni/Au and Au/Ni interface is the same in (a′) and (b′), and it is an average of the distance gradient obtained in the (a) and (b) model. The (a′) model is chemically abrupt. The (b′) model has a concentration profile given by the concentration profile of the (b) fit (see Table I). In the (a′) and (b′) models, $N_{\mathrm{Au}}=12$, $N_{\mathrm{Ni}}=5$, and $d_{\mathrm{Au}}=2.367$ Å to adjust the superperiod. Interfacial distances were calculated as in Sec. III B. We calculated the smooth part [the $\chi(E)$ dependence is omitted] of the anomalous variation of each peak using formula (3). The variations of f' and f'' used[27] in formula (3) are shown in Fig. 6.

The top anomalous intensity variations are, of course, quantitatively different for each peak depending on the (a′) and (b′) model. Nevertheless, we note that the variation of the 1^{2} and 1^{-2} peaks is qualitatively characteristic of the model used for the simulation. As one can see in Fig. 7, the shape is clearly reversed if intermixing is allowed or not. The anomalous variation of all the other peaks is quantitatively different, but the global shape is the same for the two models. Figure 7 shows the 1^{2},1^{-2} and 1^{-3},1^{1} peaks as examples. The behavior of the 1^{2} and 1^{-2} peaks gives, *a priori*, a *semiqualitative criterion* to evidence the chemical nature of the interface. For this criterion to be reliable, the characteristic shape of the DAFS spectra should be stable for a little variation of the structure. We tested the stability of all the peaks around models (a′) and (b′). The intermixing was allowed to extend from one to four planes at each side of the interface. The concentration profile gradient is linear, and the intermixed equivalent quantity ranges from one-half to two atomic planes. The stability related to the interplanar distance profile was also tested. The variations range from an abrupt interface (all distances in the Au- and Ni-rich layers are set to d_{Au} and d_{Ni}, respectively) to a maximum linear and symmetric deformation model. In this latter model, four interplanar distances at each side of the interface are modified, decreasing the Au interplanar distances and increasing the Ni

interplanar distances. The extreme deformations are *a priori* unphysical, but they allow for testing the stability of the criterion in a large range. Figure 8 shows the shape of the anomalous variation of the 1^2 and 1^{-2} peaks when one varies the structure around the (a′) and (b′) models. The anomalous variation shape of the 1^2 peak is clearly reversed when the structure is modified. Modifying the profile, the shape qualitatively goes from the shape related to the (b′) model to the shape related to the (a′) model. Misinterpretation of the actual nature of the interface can be done using the 1^2 peak. The shape of the 1^{-2} peak is modified but not reversed when the deformation or the concentration profile is changed in model (b′). In model (a′) the shape of the 1^{-2} peak is largely modified, but never seems like the shape reached in the model (b′). In conclusion, *the semiqualitative criterion is stable only for the* 1^{-2} *peak*. When variations around (a′) and (b′) are allowed, the peak top intensity, for a given q, is roughly constant except for the 1^{-2} peak (see in Fig. 8 the factors globally applied to the spectra to adjust the intensity at 8200 eV). We note that the intensity of the 1^{-2} peak is two orders of magnitude smaller when neither deformation nor intermixing is allowed. The 1^{-2} peak vanishes when the structure is abrupt. Experimentally, the 1^{-2} peak is clearly present, which means that the interface is unambiguously under deformation and/or intermixed. Moreover, we deduced from this stability study that the 1^2 peak is largely influenced by the exact interfacial distance profile and less by the exact interfacial concentration profile.

To summarize, we showed that the shape of the anomalous variation of the 1^{-2} peak is stable by considering variations of the structure and also characteristic of the actual chemical nature of the interface. Thus a reliable conclusion concerning the occurrence of intermixing can be achieved by qualitatively examining the 1^{-2} peak DAFS spectra. The refinement of the structure implies a quantitative fitting procedure and has to be simultaneously performed with anomalous variation of all the peaks (mainly with the 1^2, 1^{-2}, and 1^{-3} peaks).

B. X-ray anomalous scattering data fitting

The data normalization is done using formula (1). The K factor cannot be directly retrieved from the top-DAFS spectra. We set K to vary linearly with energy. This variation is due to experimental causes like, for example, the efficiency of the detector as a function of energy. For each peak separately, $\mu(E)$ is deduced from the fluorescence measurement. The fluorescence is normalized to match, at energies far from the Ni edge, the mean $\mu(E)$ calculated in Sec. III A. For example, Fig. 9 shows the normalized fluorescence near the 1^{-2} peak. Figure 10 shows the raw (I/I_0) and the normalized (for fluorescence and absorption) top-DAFS spectra of the 1^{-2} and 1^2 peaks. The normalization does not change the general shape of the spectra. Corrections are relatively important only for the 1^{-2}, 1^{-3}, and 1^{-4} peaks (not shown). But the relative anomalous variations of intensity are very similar after the corrections. The corrections act like a global scale factor and/or a small background effect.

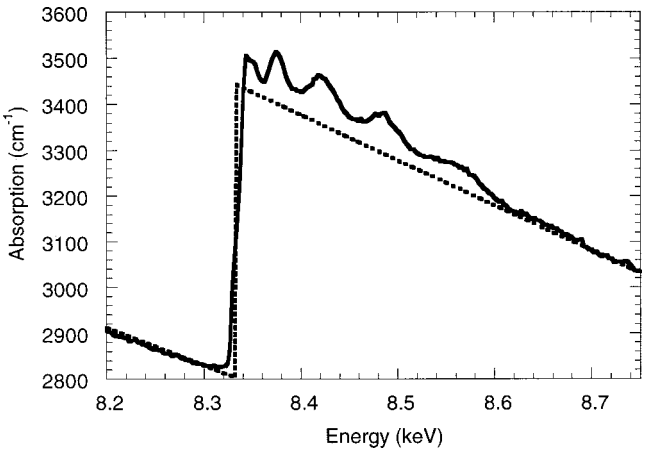

FIG. 9. The calculated absorption for Au_3Ni (dashed line). The experimental absorption extracted from the fluorescence data near the 1^2 peak and normalized, far from the edge, on the calculated one (solid line). Note that the edge crossing is softer in the experimental spectra.

Due to the shape of the anomalous variation of the 1^{-2} peak (see Fig. 7) and remembering that this shape provides a stable criterion, the interface is clearly chemically diffuse. We refined the actual structure, taking as initial conditions the structural parameters extracted from the (b) model. We chose to perform a simple fitting procedure with only two independent parameters rather than to introduce, as fitting variables, each interplanar distance and each in-plane concentration. The first parameter describes the steepness of the linear and symmetric concentration profile: the second parameter describes the steepness of a linear and symmetric

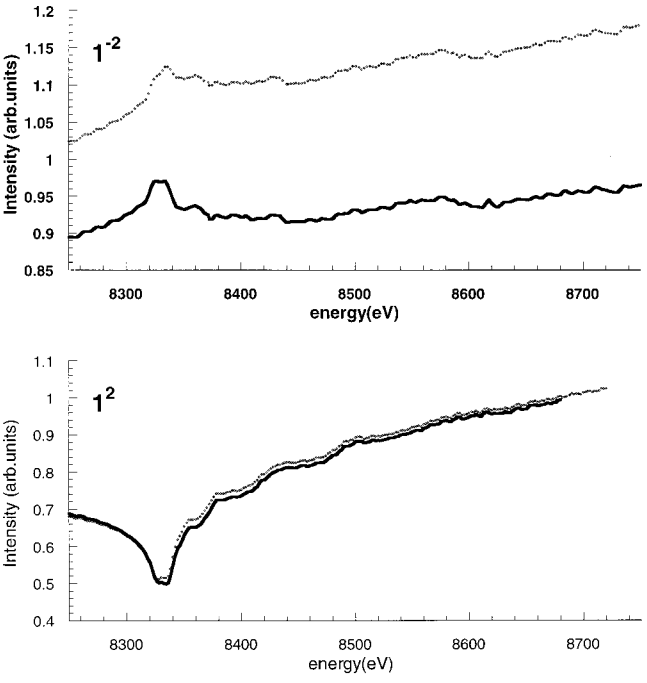

FIG. 10. Top anomalous variation of the intensity of the 1^{-2} and 1^2 peaks. Solid line: data corrected for the absorption and the fluorescence effects. Dots: raw data (I/I_0).

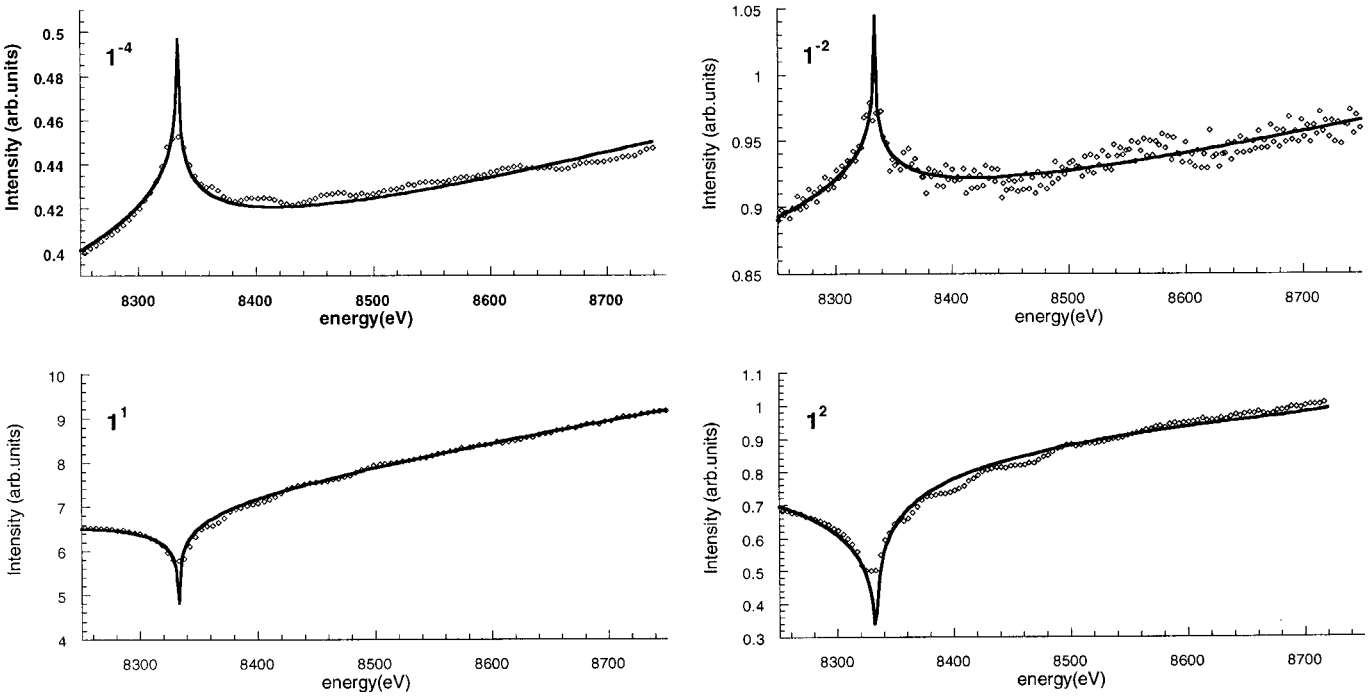

FIG. 11. Solid line: anomalous variation of the best fit (see Table II). Dots: experimental data (corrected for the absorption and fluorescence effects).

interplanar distance profile. We assume a linear interfacial profile since it is the model available in SUPREX. This shape clearly induces a limit in the fitting procedure. The main peaks can be fitted with a large number of parameter pairs. The possible solutions are clearly reduced for the weakest peaks. We deduced the best fitting structure as follows: (1) Among all the satisfying couples of parameters, we chose the ones common to all the peaks. (2) For each peak, the top-intensity ratio (at 8250 and 8750 eV) between the simulated 1^1 peak and the considered simulated peak has to be as close as possible to the corresponding experimental ratio. This latest Rietveld-like[33] constraint is very strong and limits largely the possible couples of parameters. For the best structure, most of the peaks are in good agreement with this constraint. Only the 1^{-4} peak does not satisfy the Rietveld-like constraint (the calculated ratio is 40% smaller than the experimental one). We assumed that the disorder does not explain this disagreement. We point out that in the symmetric scans (see Fig. 5), the intensity of the 1^{-4} peak was not well simulated either. The disagreement observed for the 1^{-4} peak seems to be related to the simplified (linear and symmetric) interfacial structure which was used in both (b) and (b′) models.

We also verified that the linear $K(E)$ variation is roughly the same for all the peaks. $K(E)$ is really describing an experimental variation and does not introduce any artifact in the fit.

The result of the latest combined fitting procedure is shown, as an example, for the 1^{-4}, 1^{-2}, 1^1, and 1^2 peaks (see Fig. 11). Two interplanar distances are modified on each side of the Ni/Au interface. The concentration profile extends on three planes on each side of the Ni/Au interface. The two fitting parameters were independently optimized. However, the two profiles, i.e., distance and concentration, are related through Vegard's law within an error smaller than 1.2% and 0.8% in the Au- and Ni-rich layers, respectively. The Au/Ni interface is chemically abrupt, and around this interface the interplanar distances are not modified. The smooth part of the anomalous variation is fitted with the structure given in Table II. The best fit shown in Table II is in agreement with

TABLE II. Best-fit concentration and interplanar distance profiles from the anomalous diffracted intensity. Only the interface Ni/Au is described. The number of Au and Ni planes in one bilayer is N_{Ni} and N_{Au}. The nondeformed interplanar distances (far from the interfaces) are d_{Au} and d_{Ni}. The table has to be read from the left to the right, which corresponds to the growth direction. Only the region affected by the interface presence is shown. The other distances and concentrations in the Au-rich layer are equal to d_{Au} and 100%.

n_{Au} d_{Au} (Å)	N_{Ni} d_{Ni} (Å)	Au-rich layer profile Au concentration (%) Interplanar distance (Å)	Ni-rich layer profile Ni concentration (%) Interplanar distance (Å)
12	5	..., 100; 100; 90; 74; 57.9	57.9; 74; 90, 100, 100
2.3670	2.0587	..., 2.367; 2.367; 2.3253; 2.2691	2.1565; 2.100; 2.0587; 2.0587

the (b) model of Table I. The small differences are due to the constraints assumed in the x-ray anomalous scattering analysis (mainly an integer number of planes).

The shape of the anomalous variation is globally well fitted for all peaks. Nevertheless, even for the main peaks (see the 1^1 peak, for example), which are weakly structure dependent, the crossing of the edge is always overestimated. It seems that an improvement of the structural fitting parameters (for example, a concentration and an interplanar distance for each plane) would not be sufficient to describe the actual edge. The anomalous variation of the f' and f'' factors, calculated by Sasaki[27] and used in this study, do not take into account either the finite lifetime of the core level or the true solid state. According to Ravel *et al.*,[34] the fitting can be improved by calculating refined anomalous scattering variations from the absorption data (see Fig. 9). We can clearly see in Fig. 9 that the actual absorption edge is softer than the calculated one. The f'' coefficient is given by the absorption function using the optical theorem.[35] The true f'' and the related, via Kramers-Kronig transformation, true f' could also be softer. This softening could produce a less abrupt cusp in the DAFS spectra. Nevertheless, this refinement is out of the scope of this paper and will be done in a further work.

In conclusion, the semiqualitative criterion given by the 1^{-2} peak and the results of the fitting procedure, even if the edge is not perfectly simulated, permit us to conclude unambiguously that the Au:Ni multilayers are chemically diffuse on six planes at the interface Ni/Au and are abrupt at the interface Au/Ni.

V. CONCLUSION

Different studies dealing with the (111) Au:Ni multilayers suggested an interfacial mixing to explain the behavior of the system, but until now no direct evidence was found. Our work clearly shows, using an anomalous x-ray diffraction analysis, that the Ni/Au interface is mixed, though the Au/Ni one is chemically abrupt. In the direction perpendicular to the interfaces, the concentration profile and the deformation profile were determined. We showed that the intermixed region extends on six planes at the Ni/Au interface and corresponds to two exchanged equivalent Au planes. The interplanar distance profile and the concentration profile around the Ni/Au interface satisfy Vegard's law. In the (111) Au/Ni multilayers, the asymmetric structure of the Au/Ni and Ni/Au interfaces probably indicates that the mixing is due to a gold dynamical segregation during the growth.

More generally, a fine characterization of interfaces is important in order to understand the mixing mechanism in bulk immiscible and highly mismatched multilayer systems. The combined analysis used in this work is a powerful method to study, at the atomic scale, the actual interfacial structure in nanolayered materials. We particularly showed how the x-ray anomalous diffraction analysis can unambiguously conclude on the chemical nature of buried interfaces.

ACKNOWLEDGMENTS

This work would not have been possible without the epitaxy skills of B. Gilles (LTPCM-CNRS) and A. Marty (CEA-DRFMC). It is a pleasure to acknowledge them also for many stimulating discussions.

[1] F. C. Frank and J. H. van der Merwe, Proc. R. Soc. London, Ser. A **189**, 205 (1949); J. H. van der Merwe, J. Appl. Phys. **34**, 123 (1963).

[2] J. W. Matthews and A. E. Blakeslee, J. Cryst. Growth **37**, 118 (1974).

[3] P. Muller and R. Kern, J. Cryst. Growth **146**, 193 (1995); P. Muller and R. Kern, Appl. Surf. Sci. **102**, 6 (1996).

[4] A. P. Payne, W. D. Nix, B. M. Lairson, and B. M. Clemens, Phys. Rev. B **47**, 13 730 (1993).

[5] J. Cahn, J. Hilliard, J. Chem. Phys. **28**, 258 (1958); J. Cahn, Acta Metall. **9**, 795 (1961).

[6] J. Tersoff, Phys. Rev. B **74**, 434 (1995).

[7] B. Averbach, P. Flinn, and M. Cohen, Acta Metall. **2**, 92 (1954).

[8] H. Okamoto and T. B. Massalski, *Phase Diagrams of Binary Gold Alloys* (American Society for Metals, Metals Park, OH, 1987).

[9] W. R. Tyson, Surf. Sci. **62**, 267 (1977).

[10] Y. Hiki and A. Granato, Phys. Rev. **188**, 411 (1966).

[11] S. Labat, P. Gergaud, O. Thomas, B. Gilles, and A. Marty, J. Appl. Phys. **87**, 1172 (2000).

[12] S. Baker, J. Bain, B. Clemens, and W. Nix, in *Polycrystalline Thin Films: Structure, Texture, Properties and Applications*, edited by K. Baumak, M. A. Parker, J. A. Floro, R. Sinclair, and D. A. Smith, Mater. Res. Soc. Symp. Proc. No. **343** (Materials Research Society, Pittsburgh, 1994), p. 555.

[13] K. O. Schweitz, J. Bottinger, J. Chevalier, R. Feidenhans'l, M. M. Nielsen, and F. B. Rasmussen, J. Appl. Phys. **88**, 1401 (2000).

[14] A. F. Jankowski, J. Appl. Phys. **71**, 1782 (1992).

[15] S. Labat, P. Gergaud, O. Thomas, B. Gilles, and A. Marty, Appl. Phys. Lett. **75**, 914 (1999).

[16] P. Bayle, T. Deutsch, B. Gilles, F. Lancon, A. Marty, J. Thibault, C. Colliex, and M. Tence, in *Defect-Interface Interactions*, edited by E. P. Kuan, A. H. Kang, M. J. Mills, T. D. Sands, and V. Vitek, Mater. Res. Soc. Symp. Proc. No. 319 (Materials Research Society, Pittsburgh, 1994), p. 33.

[17] H. Renevier, J. L. Hodeau, P. Wolfers, S. Andrieu, J. Weigelt, and R. Frahm, Phys. Rev. Lett. **78**, 2775 (1997).

[18] M. de Santis, A. de Andres, D. Raoux, M. Maurer, M. F. Ravet, and M. Piecuch, Phys. Rev. B **46**, 15 465 (1992).

[19] A. Barbara, J. M. Tonerre, M. C. Saint Lager, D. Raoux, S. Andrieux, M. Piecuch, E. Elkaim, and J. P. Lauriat, J. Magn. Magn. Mater. **156**, 111 (1996).

[20] D. C. Meyer, K. Richter, and P. Paufler, Phys. Rev. B **59**, 15 253 (1999).

[21] J. C. Woicik, J. O. Cross, C. E. Bouldin, B. Ravel, J. G. Pellegrino, B. Steiner, S. G. Bompardre, L. B. Sorensen, K. E. Miyano, and J. P. Kirkland, Phys. Rev. B **58**, R4215 (1998).

[22] G. M. Chow, W. C. Goh, Y. K. Hwu, T. S. Cho, J. H. Je, H. H. Lee, H. C. Kang, D. Y. Noh, C. K. Lin, and W. D. Chang, Appl. Phys. Lett. **75**, 2503 (1999).

[23] H. J. Stragier, J. O. Cross, J. J. Rehr, and L. B. Sorensen, Phys. Rev. Lett. **69**, 3064 (1992); Arcon, A. Kodre, D. Glavic, and M. Hribar, J. Phys. (Paris), Colloq. **48**, C9-1105 (1987); J. Cross, M. Newville, J. Rehr, L. Sorenson, C. Bouldin, G. Watson, T. Gouder, G. Lander, and M. Bell, Phys. Rev. B **58**, 11 215 (1998).

[24] J. L. Ferrer, J. P. Simon, J. F. Berar, B. Caillot, E. Fanchom, O. Kaikati, S. Arnaud, M. Guidotti, M. Pirochhi, and M. Roth, J. Synchrotron Radiat. **5**, 1346 (1998).

[25] E. Fullerton, I. K. Schuller, H. Vanderstraeten, and Y. Bruynseraede, Phys. Rev. B **45**, 9292 (1992).

[26] B. L. Henke, E. M. Gullikson, and J. C. Davis, At. Data Nucl. Data Tables **54**, 181 (1993).

[27] S. Sasaki (unpublished).

[28] The notation Au/Ni (Ni/Au) means the interface generated during the deposition of a Au (Ni) layer on an existent Ni (Au) layer. See also Fig. 4.

[29] W. Sevenhans, M. Gijs, Y. Bruynseraede, H. Homma, and I. K. Schuller, Phys. Rev. B **34**, 5955 (1986).

[30] G. Gladyszewski, S. Labat, P. Gergaud, and O. Thomas, Thin Solid Films **78**, 319 (1998).

[31] S. Labat, Ph.D. thesis, Université d'Aix Marseille III, 1998.

[32] M. G. Proietti, H. Renevier, J. L. Hodeau, J. Garcia, J. F. Bérard, and P. Wolfers, Phys. Rev. B **59**, 5479 (1999).

[33] L. B. McCusker, R. B. Von Dreele, D. E. Cox, D. Louer, and P. Scardi, J. Appl. Crystallogr. **32**, 36 (1999).

[34] B. Ravel, C. E. Bouldin, H. Renevier, J. L. Hodeau, and J. F. Bérard, Phys. Rev. B **60**, 778 (1999).

[35] B. Cullity, *Elements of X-Ray Diffraction*, 2nd ed. (Addison-Wesley, New York, 1978).